Size, shape, and strain dependence of the *g* factor in self-assembled In(Ga)As quantum dots

T. Nakaoka,[1] T. Saito,[2] J. Tatebayashi,[1] and Y. Arakawa[1]
[1]*Research Center for Advanced Science and Technology, University of Tokyo, Tokyo 153-8904, Japan*
[2]*Center for Collaborative Research, University of Tokyo, Tokyo 153-8904, Japan*
(Received 11 June 2004; revised manuscript received 20 August 2004; published 28 December 2004)

We have investigated Zeeman splitting in single self-assembled InAs and InGaAs quantum dots experimentally and theoretically. By measuring photoluminescence from single dots, in a wide spectral region, we have obtained the exciton *g* factors of quantum dots with various photoluminescence energies. We find that the absolute value of the exciton *g* factors of InAs dots are smaller than those of the InGaAs dots, which differs from the composition dependence expected from that of the bulk ones. The experimentally obtained *g* factors are compared with calculated ones based on the eight-band $\mathbf{k}\cdot\mathbf{p}$ model where the influence of strain and the Zeeman effect are included. We find a good agreement between the calculation and the experiment qualitatively and quantitatively. The calculation reproduces the nontrivial composition dependence of the *g* factor of the quantum dots. In addition, the eight-band model predicts a size and shape dependence of the electron and hole *g* factors of the pyramidal quantum dots.

DOI: 10.1103/PhysRevB.70.235337 PACS number(s): 73.21.−b, 71.35.−y, 71.18.+y, 71.70.Ej

I. INTRODUCTION

Self-assembled quantum dots are promising candidates for the basic device units for quantum information processing in solid state systems since the carriers can be trapped into them in a controllable manner even at relatively high temperatures[1,2] due to the strong three-dimensional confinement.[3,4] Especially, spin degrees of freedom of the confined carriers are attractive qubit candidates with relatively long decoherence times. The key quantity needed in understanding the spin effects is the *g* factor which is the coefficient connecting spin moment with magnetic one. The knowledge of electron and hole *g* factors and their control are important for spin-based quantum information applications. For example, the system with a large *g* factor is preferable for controlling spin qubit while near-zero electron *g* factor is suitable to design a quantum receiver.[5,6] The *g* factors of self-assembled dots have been evaluated by optical measurements[7–12] and transport measurements.[13–15] Generally, the electron *g* factor is deduced from transport measurements while the exciton *g* factor is deduced from optical measurements. The evaluated values of the *g* factors are much different from bulk ones[16] possibly due to size quantization, strain, and other effects. Sensitivity of the *g* factors to the spatial confinement has been predicted by theoretical studies in several types of quantum dots such as spherical, semispherical, rectangular dots, and the dots with a parabolic confinement.[17–20] In deep-etched quantum rectangular dots and wires, the dependence of the *g* factors on the dimensionality and the size of the structures have been investigated both experimentally and theoretically.[21,22] However, the roles of the size, shape, and strain on the *g* factor of self-assembled pyramidal dots have not been clear although the self-assembled quantum dots have been intensively studied due to their good optical and electrical properties which are afforded by the Stranski-Krastanov growth mode.

In this work, we study the *g* factors of InAs and InGaAs quantum dots by single dot spectroscopy and a calculation with an eight-band $\mathbf{k}\cdot\mathbf{p}$ model taking into account the strain effect and the Zeeman effect. The single dot spectroscopy permits the study of complexes formed from electrons and holes. In other words, we can separate the emission lines of single electron-hole pairs from those of multiparticle states. The separation allows the comparison of the experiment with the eight-band effective mass calculation of single particle bound states avoiding the multiparticle effects of carriers. The calculation agrees with the experiment, and predicts the dependence of the *g* factor on the size, shape, and strain in In(Ga)As pyramidal quantum dots. The results should provide insights to control the electron and hole *g* factors in pyramidal self-assembled dots.

II. EXPERIMENTS

The samples were grown on a GaAs (100) wafer at 500 °C and 76 Torr by metal organic chemical vapor deposition. The self-assembled dots grown with nominal composition $In_{0.5}Ga_{0.5}As$ and InAs are called "InGaAs" dots and "InAs" dots, respectively. Although the In content in the quantum dots might be different with nominal one due to In segregation and migration effects,[23,24] much higher In content of the InAs dots than the InGaAs dots was confirmed by photoluminescence (PL) measurement. The InAs quantum dots show the PL around 1.0 eV at 3.5 K while the InGaAs dots show the PL around 1.2 eV. Atomic force microscopy measurements of reference uncapped samples revealed the average dot diameter of 20 nm with a standard deviation of 3 nm and height of 7 nm with a standard deviation of 2 nm, as well as the areal density of about $10^{10}/cm^2$ for both the InAs and the InGaAs dots. To isolate individual quantum dots, the samples were etched by reactive ion etching into small mesa structures with lateral dimensions of about 200 nm. Magneto-PL spectroscopy up to 5 T was performed at 3.5 K in Faraday configuration. The PL was excited with the 632.8 nm line of a He-Ne laser beam focused by a microscope objective to a diameter of about 2 μm. The excitation power was limited to 10 W/cm^2 to create only a single

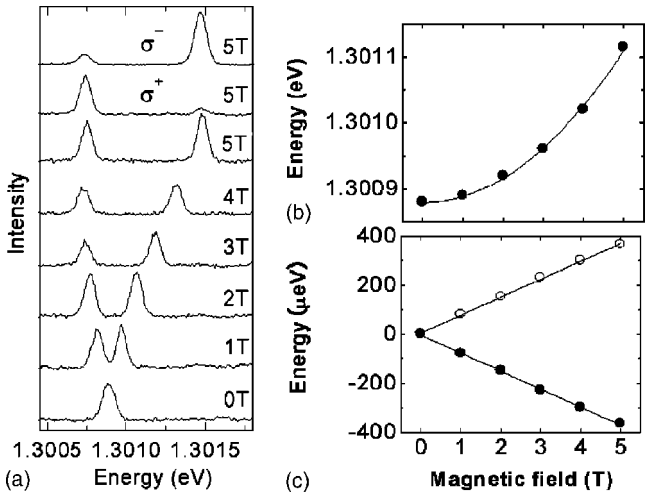

FIG. 1. (a) PL spectra of the InGaAs dots as a function of magnetic field from 0 to 5 T. All the spectra are obtained without polarization selectivity except the upper two traces that are recorded for σ^+ and σ^- circular polarizations, respectively. (b) The center position of the doublet in (a), or the diamagnetic shift, plotted as a function of magnetic field. The solid curve is a quadratic fit. (c) Peak positions after the subtraction of the diamagnetic shift, plotted as a function of magnetic field. Open (closed) circles represent the energy of σ^- (σ^+) polarized emissions. The solid lines are linear fits to the data.

electron-hole pair in a dot. The PL emission from a mesa structure was collected by the objective, dispersed by a double grating monochromator, and detected by a Si charge coupled device or an InGaAs detector array. By using these two detectors we could study the g factors in almost the whole emission energy range of the InAs and the InGaAs quantum dots.

The exciton g factor was determined by the Zeeman splitting of the ground state emissions of the single dots. We studied only the emission lines whose intensity increases linearly with excitation power in the range of 1.0–1000 W/cm^2. The emission lines are expected to arise from single neutral excitons.[25] Other lines possibly arising from complexes formed from electrons and holes were not discussed in the present work.

III. EXPERIMENTAL EVALUATION OF THE EXCITON g FACTOR

The typical PL spectra from a single InGaAs dot under applied magnetic field (B) along the growth direction are shown in Fig. 1(a). The emission lines have a linewidth of about 100 μeV. The spectral shapes of the InGaAs dots are very similar to those of the InAs dots. With increasing magnetic field, the unpolarized emission line splits into an oppositely circularly polarized doublet. The energy shift of the center of the doublet, which represents the diamagnetic shift, is quadratic in B with a constant of 9.22 μeV/T^2 [Fig. 1(b)]. The energy positions after subtracting the quadratic diamagnetic contribution shift linearly with B [Fig. 1(c)]. On the basis of the linear relationship, we define the exciton g factor as

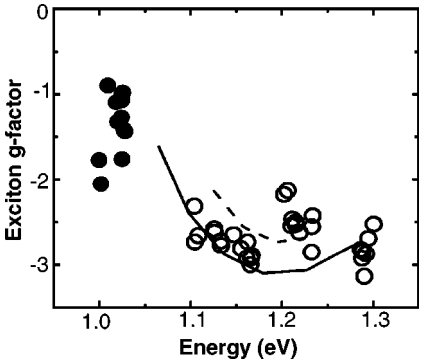

FIG. 2. Exciton g factors plotted as a function of the ground state emission energy. Open (closed) circles represent the experimental g factor of InGaAs (InAs) dots. Solid (dashed) curve gives the calculation made for the dots with a base length of 15 nm and a height of 7.5 nm (4.3 nm).

$$g_{\mathrm{ex}} = \frac{E(\sigma^+) - E(\sigma^-)}{\mu_B B}, \tag{1}$$

where $E(\sigma^+)$ and $E(\sigma^-)$ are the energies of σ^+ and σ^- polarized emissions, respectively. By fitting the data in Fig. 1(c), we obtain $g_{\mathrm{ex}}=-2.53$. We have investigated the magnetic field dependence of the emission lines for 30 InGaAs dots and 10 InAs dots, and have observed very similar magnetic field dependence for all the measured dots. All the emission lines exhibit a quadratic diamagnetic shift in addition to a linear Zeeman spin splitting into a doublet. Other features such as a zero-field splitting arising from electron-hole exchange interaction, a quadratic increase of the Zeeman splitting with B, and a splitting into a quadruplet due to an appearance of dark exciton lines have been reported[10,11] in deformed dots with broken rotational symmetry. No observation of such features suggests that most of our dots have D_{2d} symmetry except for a slight symmetry breaking due to the inequivalence of the atomic structures in the [110] and $[\bar{1}10]$ directions and the piezoelectric fields. The high symmetry of our dots is confirmed by macro-PL measurement. Although optical anisotropy has been commonly observed for elongated or asymmetric dots with C_{2v} or C_2 symmetry,[26,27] no optical anisotropy has been observed in our as-grown dots.[28]

The exciton g factors of the InAs dots and InGaAs dots obtained by the earlier-described procedure are plotted as a function of the emission energy in Fig. 2. The experimental errors are less than the size of the symbols in the figure. The scatter beyond the errors represents the inhomogeneity of the quantum dots. The exciton g factor of the InGaAs dots depends on the PL emission energy very weakly. The value ranges from −3 to −2 while that of the InAs dots ranges from −2 to −1. The compositional dependence of the g factor is different from that of the bulk materials even qualitatively. In the bulk materials, the exciton g factor of the InAs should be smaller (or the absolute value should be larger) than that of the InGaAs.[29] In order to understand the difference between the quantum dots and the bulk materials, we calculate the g factors of the quantum dots.

IV. THEORY

In this section, we describe our method to calculate the electronic properties of the InAs and InGaAs quantum dots under applied magnetic field. Our method is based on the eight-band effective mass model[30–32] which includes the conduction, heavy, light, and split-off carriers for a total of eight bands. Recently, at zero-magnetic field, the multiband effective mass model has been successfully applied to calculate pyramidal quantum dots.[33–37] We have computed the energies and wave functions by finite difference method where the material parameters and strain are varied from site to site. In the presence of a uniform magnetic field oriented along the z axis, the wave vector $\mathbf{k}$ in the effective mass Hamiltonian is replaced by the operator

$$\mathbf{k} = -i\nabla + \frac{e}{\hbar}\mathbf{A}, \tag{2}$$

where $\mathbf{A}$ is the vector potential. For the vector potential, we choose the Landau gauge

$$\mathbf{A} = -By\mathbf{x}. \tag{3}$$

The total Hamiltonian in a magnetic field is written as

$$H_{\text{tot}} = H_k + H_s + H_z, \tag{4}$$

where H_k is the kinetic piece of the effective mass Hamiltonian, H_s is the strain-dependent one, and H_z is the Zeeman Hamiltonian describing the interaction of the spin with the magnetic field. We solve the Schrödinger equation for the multicomponent spinor of the envelope functions. Following Bahder,[31] we choose Bloch functions, in the order c^-, c^+, lh^+, hh^+, hh^-, lh^-, so^-, and so^+, to represent the conduction, heavy, light, and split-off carriers, respectively. The signs $(\pm)$ on the top label the sign of the z component (J_z) of the total angular momentum $(\mathbf{J})$ formed by coupling the spin and the orbital angular momentum. Our set of the Bloch functions $|J,J_z\rangle$ and the Hamiltonans H_k, H_s, and H_z in the basis set are described in the Appendix. The Hamiltonian is discretized on a three-dimensional mesh. The dot is modeled with the shape of a pyramid with a square base of b nm and a height of h nm. The pyramid is embedded in the center of a cube with sides of 50 nm. Wetting layer is omitted in the calculation because the thickness is represented by a too small number of grids in the condition avoiding exorbitant computational expense. The wetting layer may be accounted for separately. The strain distribution in and around the dot is calculated by a three-dimensional finite element analysis employed on the modeled structure. The lattice mismatch between GaAs and $In_xGa_{1-x}As$ is incorporated through a linear static analysis. The calculated strain components are substituted for the strain Hamiltonian H_s. In addition to the explicit strain dependence in H_s, the effect of piezoelectric fields is included in the calculation. The piezoelectric polarization $\mathbf{P}_p$ in the zinc blende materials is determined as a linear function of off-diagonal components of the strain tensor ϵ_{ij}: $P_i = e_{14}(\epsilon_{jk}+\epsilon_{kj})$, $(i \neq j \neq k)$, where e_{14} is the piezoelectric constant. The electrostatic potential induced by the piezoelectric charge density $\rho = -\text{div}\mathbf{P}_p(\mathbf{r})$ is calculated by solving the corresponding Poisson equation, and is included in the Hamiltonian. The material parameters used in the calculation are summarized in Table I. All the parameters are set to the values corresponding to the local composition except for the dielectric constant which is set to the value for the dot composition throughout the structure. The discretized Hamiltonian is diagonalized by the Arnoldi-Lanczos algorithm.

TABLE I. Material parameters used in the calculation. Unless otherwise noted, values are taken from Ref. 44.

Quantity	$In_xGa_{1-x}As$
Deformation potentials	
a_c (eV)	$-5.08x-7.17(1-x)$
a_v (eV)	$-1.00x-1.16(1-x)$
b_v (eV)	$-1.8x-2.0(1-x)$
d_v (eV)	$-3.6x-4.8(1-x)$
Energy gap	
E_g (eV)	$0.417x+1.519(1-x)-0.477x(1-x)$
VB offset	
E_{vbo} (eV)	$0.21x+0.38x(1-x)$
Luttinger parameters	
γ_1^L	$20.0x+6.98(1-x)$
γ_2^L	$8.5x+2.06(1-x)$
γ_3^L	$9.2x+2.93(1-x)$
κ^L	$7.68x+1.20(1-x)$[a]
Spin-orbit coupling energy	
Δ_{so} (eV)	$0.39x+0.341(1-x)-0.15x(1-x)$
Optical matrix parameter	
E_P (eV)	$21.5x+28.8(1-x)+1.48x(1-x)$
Static dielectric constant	
ϵ_s	$15.15x+13.18(1-x)$[b]
Piezoelectric modulus	
e_{14} (C/m^2)	$-0.05x-0.16(1-x)$[b]

[a]Reference 6.
[b]Reference 45.

V. NUMERICAL RESULTS AND COMPARISON WITH EXPERIMENT

In absence of magnetic fields, the calculated result is very similar to previously reported eight-band $\mathbf{k}\cdot\mathbf{p}$ calculations.[33–37] The ground lowest conduction band (CB) state is always s-like, and is mostly localized in the middle of the pyramidal dot structure. The projection of the wave function to the s-like Bloch function $(c^{\pm})$ is more than 90% in all the calculated dots although the shape is slightly elongated along the diagonal direction of the square base due to the piezoelectric potential. The first and second excited states (labeled ignoring the Kramers degeneracy at the zero magnetic field) are p-like, and are splitted also due to the piezoelectric potential. On the other hand, the ground valence band (VB) state remains closer to the bottom. Most hole states are elongated and localized along the diagonal direction of the dot square. The projection of the hole wave function to the bulk heavy hole (HH) band $(hh^{\pm})$ is more than 80% in all the

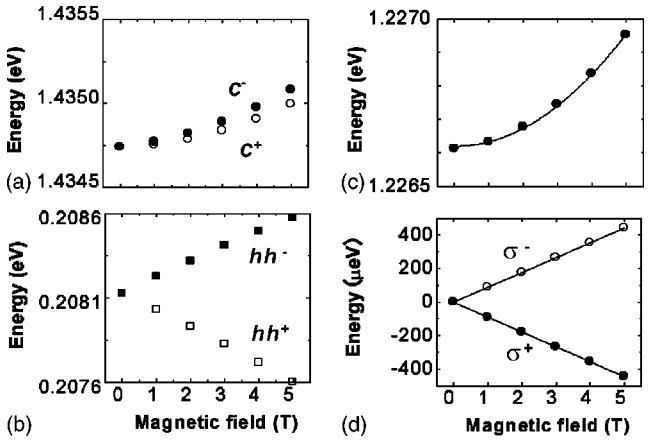

FIG. 3. Magnetic field dependence of the energy of (a) the lowest CB state and (b) the highest VB state. The zero of the energy scale is taken at the VB edge of unstrained GaAs. (c) Magnetic field dependence of the calculated energy of the center of the spin-splitted transition energies. The solid curve shows a quadratic fit to the calculated energies. (d) Magnetic field dependence of the calculated transition energies of σ^+ polarized emission (closed symbols) and σ^- polarized emission (open symbols). The solid lines are linear fits to the data.

calculated dots. In the following, we label the calculated ground states by using the dominant components of the Bloch functions, namely, c^+, c^-, hh^+, and hh^-. We note that the size-dependence of the calculated energy levels in the InAs pyramidal dots with (101) facets is also very similar to previously reported ones[33,35] except for slight differences possibly due to different material parameters used for the calculation. For example, the splitting magnitude between the *p*-like electron states and the energy separation between the first and the second excited hole states are rather close to the values reported in Ref. 33 than those in Ref. 35.

Figures 3(a) and 3(b) show the calculated energies of the the lowest CB state and the highest VB state under applied magnetic field. The calculated dot has a pyramidal shape with a height of 7.5 nm, a base width of 15 nm, and a diagonal length of 21.2 nm. The pyramidal shape with a diagonal length of 21.2 nm is adopted to compare the measured dots with a diameter of 20 nm on average although the atomic force microscopy is not capable of resolving the detailed dot shape due to the tip-convolution effect. The composition $In_{0.6}Ga_{0.4}As$ of the calculated dot may be representative of the measured InGaAs dots with the nominal composition of $In_{0.5}Ga_{0.5}As$. The size and composition dependence of the magneto-optical properties will be discussed later in more detail.

When we apply a magnetic field, the Kramers degenerate states of the calculated CB and VB states split into doublets due to the Zeeman effect. We focus on the Zeeman splitting of the ground states although the eight-band calculation gives also the splittings of the excited states, which are much larger than those of the ground states due to nonzero mesoscopic angular momentum.[38] To compare the calculated results with the experiment, we derive the emission energy from the the calculated energies of the CB and VB states. The emission of a photon occurs from the interband optical transition from a single electron state of the CB to an empty single-electron state of the VB, which is related to the single-hole state by time reversal. Therefore, in the dipole approximation, the transition energy of σ^+ (σ^-) polarized emission is obtained from the energy difference between the c^- (c^+) CB state and the hh^- (hh^+) VB state if we neglect the *e-h* Coulomb interaction. The effect of *e-h* Coulomb interaction on magneto-optical properties[39] can be discussed independently in a weak magnetic field range where modification of the exciton wave function induced by the magnetic field is very small. In our calculation, the projections of the CB and the VB states to their dominant components of the Bloch functions vary by less than 1% in the range of magnetic field from 0 to 5 T. Thus, the *e-h* Coulomb interaction does not significantly change the *g* factor in our condition. The effect can be included by just adding the exciton binding energy of several tens of milli-electron-volts although we neglect it for simplicity.

The center of the calculated energies of the σ^+ and σ^- polarized emissions, which represents the diamagnetic shift, is shown in Fig. 3(c). The energy can be fitted well by a quadratic function of B with a constant of 13.8 $\mu eV/T^2$. Thus, the calculation reproduces well the quadratic diamagnetic shift measured by the single dot spectroscopy. Figure 3(d) shows the transition energy of the σ^+ and σ^- polarized emissions after subtracting the energy of the center of the emissions. The linear Zeeman splitting is also reproduced. It should be noted that, strictly speaking, the calculated diamagnetic shift is not exactly quadratic in B and the calculated Zeeman splitting is not strictly proportional to B due to the weak modification of $\mathbf{k}\cdot\mathbf{p}$ coupling by the magnetic field. We determine the exciton *g* factor by fitting the Zeeman splitting with a linear function as $E(\sigma^+)-E(\sigma^-)=g_{ex}\mu_B B$. Thus, we obtain the exciton *g* factor for dots with various composition, size, and shape.

The composition dependence of the exciton *g* factor of the dots with a base width of 15 nm (diagonal length of 21.2 nm) and a height of 7.5 nm is compared to the experiment for the dots with a diameter of 20 nm and a height of 7 nm in Fig. 2 by plotting the *g* factor as a function of the emission energy. The dot composition is represented by the corresponding ground-state transition energy. The lowest emission energy pertains to the InAs dot while the highest emission energy to the $In_{0.5}Ga_{0.5}As$ dot. In addition to the *g* factors of the dots with a height of 7.5 nm, those of the dots with a height of 4.3 nm are also shown since the capping of GaAs barrier layer might reduce the height of the dot by several nanometers.[40] In the dot structure the highest emission energy pertains to $In_{0.7}Ga_{0.3}As$ dot. With further increasing Ga content, electrons are not confined in the dots. Figure 2 shows a good agreement between the experiment and the calculation. Not only the quantitative values of the exciton *g* factors, but also the characteristic composition dependence of the *g* factor, namely the smaller absolute values of the *g* factors of the InAs dots than those of the InGaAs dots, is well reproduced. In the following we discuss the characteristic composition dependence.

The exciton *g* factor is written by $g_{ex}=-g_c+g_v$, when we define the *g* factors of the lowest CB state and the highest VB state as $g_c \equiv (E(c^+)-E(c^-))/(\mu_B B)$, and $g_v \equiv [E(hh^+)$

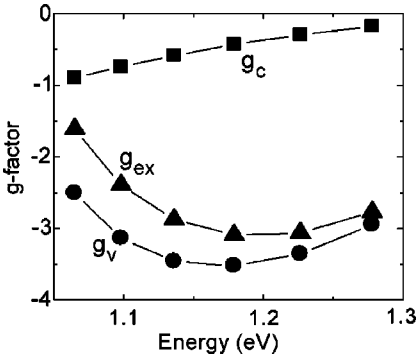

FIG. 4. Calculated g factors of the lowest CB state (g_c), the highest VB state (g_v), and the electron-hole pair (g_{ex}), as a function of the emission energy of the quantum dots with a base length of 15 nm and a height of 7.5 nm. The lines are to guide the eye. The composition of the quantum dots, ranging from pure InAs to $In_{0.5}Ga_{0.5}As$, are represented by the emission energy.

$-E(hh^-)]/(\mu_B B)$, respectively. It may be noted that hole g factor has opposite sign to g_v. As shown in Fig. 4, in the dots with a base length of 15 nm and a height of 7.5 nm, the variation of g_v with composition is much larger than that of g_c. Therefore, the compositional variation of g_{ex} is dominated by g_v. It should be noted that the characteristic composition dependence cannot be explained by the wave function spill-over from the In(Ga)As dot to the GaAs barrier layer. More than 95% of the hole wave function is always confined in each dot in all the calculated compositions.

The VB g factor g_v is strongly influenced by the $k\cdot p$ coupling. We have confirmed that if the $k\cdot p$ coupling among the VBs ($hh^{\pm}$, $lh^{\pm}$, and $so^{\pm}$) is neglected by setting the corresponding off-diagonal elements are set to zero, then the characteristic compositional dependence vanishes to approach the bulk g factor qualitatively and quantitatively. An important contribution for the $k\cdot p$ coupling arises from the shear strain in and around the dot since the off-diagonal components of the strain Hamiltonian H_s are composed mainly of the shear strain components.[30,31] The shear strain decreases with increasing Ga content. The decrease of the shear strain decreases the $\mathbf{k}\cdot\mathbf{p}$ coupling, and results in an increase of the HH band projection. The increase of the HH band projection increases the absolute value of the g factor because the HH band is fully perpendicular to the magnetic field while the light hole and split-off bands have a parallel component to the magnetic field. Thus, with increasing Ga content, the relaxation of the shear strain increases the absolute g factor value despite the decrease of its bulk value. In contrast to the good agreement of the g factor with experiment, the calculated emission energy is slightly different from the experiment. The slight disagreement may be improved by finely tuning the dot shape, and by taking into account nonuniformity of In distribution[23] although the characteristic magneto-optic properties of the self-assembled In(Ga)As quantum dots are well reproduced in our simple model structure.

VI. SIZE AND SHAPE DEPENDENCE OF THE g FACTOR

By using the same calculation procedure which gives the good agreement with the experiment, we study the size and

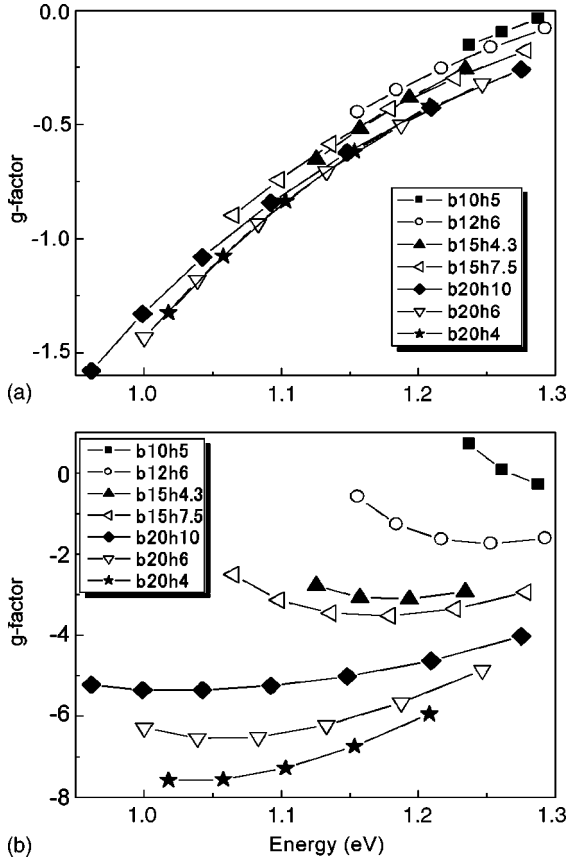

FIG. 5. Calculated g factors of (a) the lowest CB state and (b) the highest VB state for quantum dots with various size and shape, plotted as a function of the emission energy. The dot size and shape are labeled by the base length (b nm) and the height (h nm). The composition of the quantum dots, ranging from pure InAs to maximum allowable Ga-rich InGaAs for carriers to be confined, are represented by the emission energy.

shape dependence of the g factors. The g factors of the lowest CB state (g_c) and the highest VB state (g_v) in the quantum dots with various shape and size are shown in Fig. 5. The dot composition is represented by the corresponding emission energy. The composition dependence of the CB g factor is very similar in all the dots. The g factor depends mainly on the emission energy although there is a tendency for the absolute g factor value to increase with increasing size. This is due to increased orbital contribution to the g factor through decreased quantum confinement. In other words, electrons in a strongly confined quantum dot stay in its ground orbital state. Strong quantum confinement pushes the CB g factor toward 2. On the other hand, the composition dependence of the VB g factor strongly depends on the size and the shape. First, we focus on the dot-size variation of $|g_v|$, keeping the base-to-height ratio $b/h=2$ in the dots with a base length ranging from 10 to 20 nm. The dots are labeled by their base width (b nm) and height (h nm) as b10h5, b12h6, b15h7.5, and b20h10. In all the compositions of the dots, the absolute g factor value $|g_v|$ decreases with decreasing dot size, due to decreased orbital contribution. In addition, with decreasing dot size, the characteristic composition dependence becomes strong. In the small dots, the absolute g

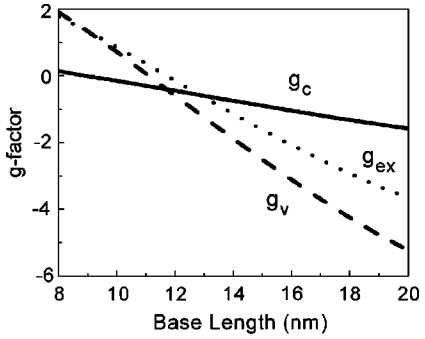

FIG. 6. Size dependence of the g factors in the pyramidal InAs dots with a base to height ratio of 2.

factor value increases largely with the emission energy or with the Ga content. It should be noted here that the eight-band $\mathbf{k}\cdot\mathbf{p}$ theory is accurate in the vicinity of the Γ point. The accuracy of the eight-band model decreases for smaller dots and more elaborate methods as empirical pseudopotential calculations are necessary. Comparison for InAs quantum dots have shown a reasonable agreement between eight-band $\mathbf{k}\cdot\mathbf{p}$ and the pseudopotential calculations[41] for dot base lengths $b>9$ nm.[34] In the size range, the contributions of large-$|\mathbf{k}|$ states are found to be negligible.

Next, we focus on the dot-shape variation of $|g_v|$, keeping the dot base length $b=20$ nm. The dots are labeled as b20h10, b20h6, and b20h4. With decreasing dot-height from 10 to 4 nm, the absolute g factor value increases. This is due to the increase of the HH character by decreasing the dot height or flattening the dot shape. Indeed, the HH band projection in the InAs dots increases from 84.8% to 96.8% by the height reduction from 10 to 4 nm. On the other hand, the absolute g factor values of the dots with a base length of 15 nm are slightly decreased by the height reduction from 7.5 to 4.3 nm although the HH characters are increased by the height reduction. This is because the height reduction in the dots with a base length of 15 nm induces the effect of size reduction in addition to the effect of the shape flattening. A competition between the decrease of $|g_v|$ due to the dot-size reduction and the increase due to the dot-flattening results in the slight decrease in the absolute g factor.

More detailed size dependence of the g factors in the pyramidal InAs quantum dots with (101) facets with a constant aspect ratio of 2 is shown in Fig. 6. The size dependence is close to linear although the gradients are different between the CB and VB g factors. Consequently, the g factors becomes zero and change their sign at different dot sizes.

VII. CONCLUSIONS

We have investigated the Zeeman splitting in self-assembled In(Ga)As quantum dots by single dot spectroscopy and eight-band $\mathbf{k}\cdot\mathbf{p}$ calculation. By using single dot spectroscopy we have evaluated the exciton g factors for various InAs and InGaAs quantum dots avoiding multiparticle effects as much as possible. The composition dependence of the self-assemble dots is different from the bulk ones. The absolute values of the exciton g factors of the InAs dots are smaller than those of the InGaAs dots. The characteristic composition dependence of the g factor is reproduced by the calculation based on the eight-band $\mathbf{k}\cdot\mathbf{p}$ model including strain, piezoelectric fields, and Zeeman effects. The numerically calculated g factor agrees with the experiment qualitatively and quantitatively. The eight-band calculation predicts an increase of the absolute values of the CB and the VB g factors with increasing dot size. The absolute value of the VB g factor increases with flattening the dot shape. These composition, size, and shape dependencies are attributed to the $\mathbf{k}\cdot\mathbf{p}$ coupling. Shear strain in and around the quantum dots plays an important role on the coupling. The variation of the HH projection is especially important for the VB g factor. Due to the difference of the size dependent $\mathbf{k}\cdot\mathbf{p}$ coupling between the CB state and the VB state, the CB and the VB g factors become zero and change the sign at different dot sizes. Such a controllability of the g factors may be advantageous for future quantum information processing.

ACKNOWLEDGMENTS

The authors thank T. Sato and S. Tarucha for fruitful discussions and T. Kakitsuka for assistance in the calculations. This work was supported in part by the Focused Research and Development Project for the Realization of the World's Most Advanced IT Nation, IT Program, MEXT, and also by Grant-in-Aid for COE Research (No. 12CE2004 "Control of Electrons by Quantum Dot Structures and Its Application to Advanced Electronics").

APPENDIX: BLOCH FUNCTIONS AND HAMILTONIANS

The set of Bloch functions $|J,J_z\rangle$ at the zone center is written as[31]

$$|1\rangle = \left|\frac{1}{2},-\frac{1}{2}\right\rangle = |S\downarrow\rangle, \tag{A1}$$

$$|2\rangle = \left|\frac{1}{2},\frac{1}{2}\right\rangle = |S\uparrow\rangle, \tag{A2}$$

$$|3\rangle = \left|\frac{3}{2},\frac{1}{2}\right\rangle = -\frac{i}{\sqrt{6}}|(X+iY)\downarrow - 2Z\uparrow\rangle, \tag{A3}$$

$$|4\rangle = \left|\frac{3}{2},\frac{3}{2}\right\rangle = \frac{i}{\sqrt{2}}|(X+iY)\uparrow\rangle, \tag{A4}$$

$$|5\rangle = \left|\frac{3}{2},-\frac{3}{2}\right\rangle = -\frac{i}{\sqrt{2}}|(X-iY)\downarrow\rangle, \tag{A5}$$

$$|6\rangle = \left|\frac{3}{2},-\frac{1}{2}\right\rangle = \frac{i}{\sqrt{6}}|(X-iY)\uparrow + 2Z\downarrow\rangle, \tag{A6}$$

$$|7\rangle = \left|\frac{1}{2},-\frac{1}{2}\right\rangle = \frac{i}{\sqrt{3}}|-(X-iY)\uparrow + Z\downarrow\rangle, \tag{A7}$$

$$|8\rangle = \left|\frac{1}{2},\frac{1}{2}\right\rangle = \frac{-i}{\sqrt{3}}|(X+iY)\downarrow + Z\uparrow\rangle, \tag{A8}$$

corresponding to electron spin down, electron spin up, light hole spin up, heavy hole spin up, heavy hole spin down, light hole spin down, split-off hole spin down, and up. The effective mass Hamiltonians H_k and H_s in the basis set in bulk zinc-blende materials have been given explicitly.[30,31] We use the same Hamiltonians H_k and H_s as in Ref. 31 except for the replacement of the wave vector to the operator $\mathbf{k}=-i\nabla + (e/\hbar)\mathbf{A}$ under a magnetic field $\mathbf{B}=\mathrm{rot}\mathbf{A}$. The Zeeman Hamiltonian H_z is written as[32,42,43]

$$H_z = 2\mu_B B \begin{bmatrix} -\frac{1}{2} & & & & & & & \\ & \frac{1}{2} & & & & & & \\ & & -\frac{1}{2}\kappa & & & & & -\frac{1}{\sqrt{2}}(\kappa+1) \\ & & & -\frac{3}{2}\kappa & & & & \\ & & & & \frac{3}{2}\kappa & & & \\ & & & & & \frac{1}{2}\kappa & -\frac{1}{\sqrt{2}}(\kappa+1) & \\ & & & & & -\frac{1}{\sqrt{2}}(\kappa+1) & \kappa+\frac{1}{2} & \\ & & -\frac{1}{\sqrt{2}}(\kappa+1) & & & & & -\left(\kappa+\frac{1}{2}\right) \end{bmatrix}. \tag{A9}$$

where μ_B is the Bohr magneton. The constant κ is the modified Luttinger parameter related to the Luttinger parameter by

$$\kappa = \kappa^L - \frac{1}{2}\frac{E_P}{3E_g + \Delta_{so}}, \tag{A10}$$

where E_P is the optical matrix parameter, E_g is the band gap, and Δ_{so} is the spin-orbit coupling energy.

[1] T. Lundstrom, W. Schoenfeld, H. Lee, and P. M. Petroff, Science **286**, 2312 (1999).

[2] T. Sato, T. Yamaguchi, W. Izumida, S. Tarucha, H. Z. Song, T. Miyazawa, Y. Nakata, T. Ohshima, and N. Yokoyama, Physica E (Amsterdam) **21**, 506 (2004).

[3] Y. Arakawa and H. Sakaki, Appl. Phys. Lett. **40**, 939 (1982).

[4] D. Bimberg, M. Grundmann, and N. N. Ledentsov, *Quantum Dot Heterostructures* (Wiley, New York, 1999).

[5] R. Vrijen and E. Yablonovitch, Physica E (Amsterdam) **10**, 569 (2001).

[6] A. A. Kiselev, K. W. Kim, and E. Yablonovitch, Phys. Rev. B **64**, 125303 (2001).

[7] Y. Toda, S. Shinomori, K. Suzuki, and Y. Arakawa, Appl. Phys. Lett. **73**, 517 (1998).

[8] M. Bayer, A. Kuther, A. Forchel, A. Gorbunov, V. B. Timofeev, F. Schäfer, J. P. Reithmaier, T. L. Reinecke, and S. N. Walck, Phys. Rev. Lett. **82**, 1748 (1999).

[9] M. Bayer, A. Kuther, F. Schäfer, J. P. Reithmaier, and A. Forchel, Phys. Rev. B **60**, R8481 (1999).

[10] M. Bayer, G. Ortner, O. Stern, A. Kuther, A. A. Gorbunov, A. Forchel, P. Hawrylak, S. Fafard, K. Hinzer, T. L. Reinecke, S. N. Walck, J. P. Reithmaier, F. Klopf, and F. Schäfer, Phys. Rev. B **65**, 195315 (2002).

[11] J. J. Finley, D. J. Mowbray, M. S. Skolnick, A. D. Ashmore, C. Baker, A. F. G. Monte, and M. Hopkinson, Phys. Rev. B **66**, 153316 (2002).

[12] A. R. Goñi, H. Born, R. Heitz, A. Hoffmann, C. Thomsen, F. Heinrichsdorff, and D. Bimberg, Jpn. J. Appl. Phys., Part 1 **39**, 3907 (2000).

[13] A. S. G. Thornton, T. Ihn, P. C. Main, L. Eaves, and M. Henini, Appl. Phys. Lett. **73** 354 (1998).

[14] M. C. Bodefeld, R. J. Warburton, K. Karrai, and J. P. Kotthaus, G. Medeiros-Ribeiro, and P. M. Petroff, Appl. Phys. Lett. **74** 1839 (1999).

[15] G. Medeiros-Ribeiro, E. Ribeiro, and H. Westfahl, Jr., Appl. Phys. A: Mater. Sci. Process. **77**, 725 (2003).

[16] H. Kosaka, A. A. Kiselev, F. A. Baron, K.-W. Kim, and E. Yablonovitch, Electron. Lett. **37**, 464 (2001).
[17] D. A. Broido, A. Cros, and U. Rössler, Phys. Rev. B **45**, 11 395 (1992).
[18] T. Darnhofer and U. Rössler, Phys. Rev. B **47**, 16 020 (1993).
[19] A. A. Kiselev, E. L. Ivchenko, and U. Rössler, Phys. Rev. B **58** 16 353 (1998).
[20] S. J. Prado, C. Trallero-Giner, A. M. Alcalde, V. López-Richard, and G. E. Marques, Phys. Rev. B **69**, 201310 (2004).
[21] M. Bayer, V. B. Timofeev, T. Gutbrod, A. Forchel, R. Steffen, and J. Oshinowo, Phys. Rev. B **52**, R11 623 (1995).
[22] R. Kotlyar, T. L. Reinecke, M. Bayer, and A. Forchel, Phys. Rev. B **63**, 085310 (2001).
[23] J. Shumway, A. J. Williamson, A. Zunger, A. Passaseo, M. DeGiorgi, R. Cingolani, M. Catalano, and P. Crozier, Phys. Rev. B **64**, 125302 (2001).
[24] N. Liu, J. Tersoff, O. Baklenov, A. L. Holmes, Jr., and C. K. Shih, Phys. Rev. Lett. **84**, 334 (2000).
[25] It should be noted that the charged excitons formed due to residual background doping which can occur even in nominally undoped structures may show such a linear power dependence. However, the exciton *g* factor should be identical to that of a neutral exciton, as long as the electronic band structure is identical to that of an uncharged dot. If the impurity or the dopant is located near the dot, the excitation power dependence of the emission spectra and the *g* factor should be changed largely (see Ref. 9). However, we did not observe such large variations in the magneto-optic spectra.
[26] Y. Nabetani, T. Ishikawa, S. Noda, and A. Sasaki, J. Appl. Phys. **76**, 347 (1994).
[27] M. Sugisaki, H.-W. Ren, S. V. Nair, K. Nishi, S. Sugou, T. Okuno, and Y. Masumoto, Phys. Rev. B **59**, R5300 (1999).
[28] T. Nakaoka, S. Kako, S. Ishida, M. Nishioka, and Y. Arakawa, Appl. Phys. Lett. **81**, 3954 (2002).
[29] The exciton *g* factor of bulk materials is mainly determined by the hole *g* factor. The *g* factor for heavy hole subband for a bulk zinc blende material is written as $-6\kappa^L(0)$, on the basis of the eight band $k\cdot p$ Zeeman Hamiltonian given in the text. Using the value shown in Table I, one easily finds that the absolute value of the exciton *g* factor in InAs is larger than in GaAs.
[30] J. M. Luttinger, Phys. Rev. **102**, 1030 (1956).
[31] T. B. Bahder, Phys. Rev. B **41**, 11 992 (1990).
[32] C. K. Pidgeon and R. N. Brown, Phys. Rev. **146**, 575 (1966).
[33] O. Stier, M. Grundmann, and D. Bimberg, Phys. Rev. B **59**, 5688 (1999).
[34] O. Stier, in *Nano-Optoelectronics*, edited by M. Grundmann (Springer-Verlag, Berlin, 2002), p. 167.
[35] C. Pryor, Phys. Rev. B **57**, 7190 (1998).
[36] W. Sheng and J.-P. Leburton, Phys. Status Solidi B **237**, 394 (2003).
[37] W. Sheng and J.-P. Leburton, Phys. Rev. B **67**, 125308 (2003).
[38] M. Brasken, M. Lindberg, and J. Tulkki, Phys. Rev. B **55**, 9275 (1997).
[39] K. L. Janssens, F. M. Peeters, and V. A. Schweigert, Phys. Rev. B **63**, 205311 (2001).
[40] F. Ferdos, S. Wang, Y. Wei, M. Sadeghi, Q. Zhao, and A. Larsson, J. Cryst. Growth **251**, 145 (2003).
[41] L.-W. Wang, J. Kim, and A. Zunger, Phys. Rev. B **59**, 5678 (1999).
[42] G. L. Bir and G. Pikus, *Symmetry and Strain-Induced Effects in Semiconductors* (Wiley, New York, 1974).
[43] G. D. Sanders, Y. Sun, F. V. Kyrychenko, C. J. Stanton, G. A. Khodaparast, M. A. Zudov, J. Kono, Y. H. Matsuda, N. Miura, and H. Munekata, Phys. Rev. B **68**, 165205 (2003).
[44] I. Vurgaftmann, J. R. Meyer, and L. R. Ram-Mohan, J. Appl. Phys. **89**, 5815 (2001).
[45] J. Singh, *Electronic and Optoelectronic Properties of Semiconductor Structures* (Cambridge University Press, Cambridge, 2003).